



# Effects of molecular shapes, molecular weight, and types of edges on peak positions of C1s X-ray photoelectron spectra of graphene-related materials and model compounds

Kumiko Mori<sup>1,\*</sup>, Jungpil Kim<sup>2</sup>, Shingo Kubo<sup>3</sup>, and Yasuhiro Yamada<sup>4,\*</sup> 

<sup>1</sup>Soft Molecular Activation Research Center, Chiba University, 1-33 Yayoi, Inage, Chiba 263-8522, Japan

<sup>2</sup>Carbon & Light Materials Application Research Group, Korea Institute of Industrial Technology, 222 Palbok-ro, Deokjin-gu, Jeonju 54853, Republic of Korea

<sup>3</sup>Research Support Center, Kagoshima University, 1-21-40 Korimoto, Kagoshima 890-0065, Japan

<sup>4</sup>Graduate School of Engineering, Chiba University, 1-33 Yayoi, Inage, Chiba 263-8522, Japan

**Received:** 25 March 2022

**Accepted:** 28 July 2022

**Published online:**  
25 August 2022

© The Author(s), under exclusive licence to Springer Science+Business Media, LLC, part of Springer Nature 2022

## ABSTRACT

Nanocarbon materials such as graphene and graphene nanoribbons (GNRs) have been studied for various applications such as electrodes and catalysts. For precise analyses of nanocarbon materials, analyses other than conventionally used analyses such as Raman and infrared spectroscopies and microscopies are essential. C1s X-ray photoelectron spectroscopy (XPS) is one of the general techniques used to analyze the structures of carbon materials. However, XPS has not been commonly utilized to investigate the structures of carbon materials in detail. In this work, the relevance of molecular shapes, molecular sizes, and types of edges on peak positions of C1s XPS spectra were revealed. For example, adjusted peak positions of C1s spectra of rectangular graphene-like structures such as GNRs tended to be higher than those of triangle or hexagonal graphene-like structures at the same atomic ratio of H/C mainly because rectangular structures of GNRs enhanced the conjugation more than those of hexagonal and triangle structures of graphene-related materials. Besides, the structures of graphene-related materials, such as rectangular with either zigzag or armchair edges, triangle, hexagonal, and the other structures, can be estimated without using a microscope by measuring combustion elemental analysis, mass spectrometry, C1s XPS spectra, and the highest occupied molecular orbital and comparing them with the tendencies of H/C ratio and molecular weight versus adjusted peak positions of C1s XPS spectra. Moreover, the reasons for the shift and the broadening of experimental C1s XPS spectra have been revealed to be

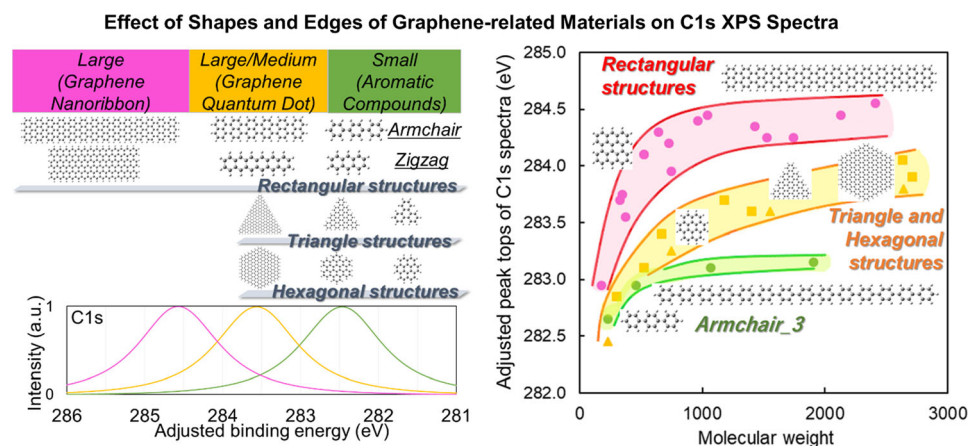
Handling Editor: Gregory Rutledge.

Address correspondence to E-mail: k.mori@chiba-u.jp; y-yamada@faculty.chiba-u.jp

<https://doi.org/10.1007/s10853-022-07599-6>

the charge-up effect caused by the large size of the powder of analyzed compounds.

## GRAPHICAL ABSTRACT



## Introduction

Nanocarbon materials such as graphene [1], carbon nanotubes [2, 3], and graphene nanoribbons (GNRs) [4] with high conductivity, specific surface area, and chemical resistance have been applied for various researches such as electrodes, catalysts, heat dissipation materials, and electromagnetic shielding materials [5–13]. The performance of nanocarbon materials for various applications has been known to be influenced by the amount and the types of edges of nanocarbon materials [14–18]. Besides, it is known that zigzag edges are electronically rich and more reactive than armchair edges [18–22]. It is also known that the width of GNRs and the size of polyaromatic hydrocarbons affect the bandgap [22–27]. Thus, understanding the shapes such as hexagonal, rectangular, and triangle (Fig. 1 ai), the molecular weight, the types of edges such as zigzag edges, which are similar to Solo, armchair edges, which are similar to Duo, Trio, Quartet/Quatro, and Quintet [28–37] (Fig. 1 aii) of nanocarbon materials are essential for the research of nanocarbon materials.

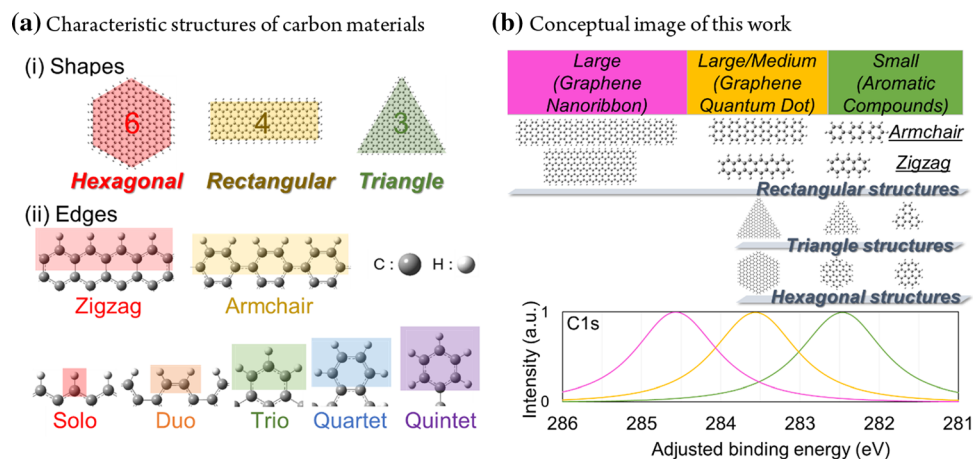
Various graphene-related materials with different shapes such as hexagonal [38–42], rectangle (GNRs)

[43–46], triangle [47, 48], circular [40, 42], star-like structures [42], and the other shapes [49–52] have been intensively studied for the last two decades. Atomic-level observations by scanning tunneling microscope [19, 20, 43, 44, 47] and transmission electron microscope with aberration corrector [53–56] have been performed to analyze edges and the other defects of nanocarbon materials. However, microscopes can only analyze the small region at the atomic scale and the determination of the bonding states is another challenge [53, 56]. In contrast, some evaluation methods such as infrared-ray (IR) [21, 45, 57–63], Raman [21, 22, 45, 63–67], nuclear magnetic resonance [45, 68–72], and X-ray photoelectron spectroscopy (XPS) [22, 23, 71–75] have been studied to analyze carbon materials precisely by combining especially with calculation because these methods can analyze the large region and the averaged information of edge structures can be readily obtained.

Among these analytical techniques, XPS is one of the essential chemical state analyses to estimate structures of carbon materials. XPS has been generally utilized to analyze the functional groups of carbon materials [71–79], metal complex [80, 81], and some defects such as  $sp^3C$  [73, 82], point defects

**Figure 1** Structures of carbon materials and conceptual image of this work.

**a** Characteristic structures of carbon materials. (1) Shapes. (2) Edges. **b** Conceptual image of this work whose peak positions of C=C were adjusted by shifting HOMO at 0 eV. (A color version of this figure can be viewed online).



[73, 83], Stone-Thrower-Wales defects [73, 83], pentagons [63, 77, 84, 85], and heptagons [71, 85, 86]. However, XPS has not been generally utilized to determine the edge structures and aromaticity except for our recent work [22, 23, 85]. As related research to this work, the aromaticity of coals has been investigated, but only the  $\pi$ - $\pi^*$  shape-up peaks were investigated [87]. The broadness of C1s XPS spectra of anthracene-based graphite has been explained to be related to the defect peaks at ca. 285 eV which is shifted from 284.6 eV of  $sp^2C$ , but the origin of the defect peaks has not been discussed in detail [88]. The C1s XPS spectra of aromatic compounds with different sizes such as coronene, circumpyrene, and circumcoronene have been studied, but the peak positions have been reported to be similar to each other [89] probably because of the calculation without consideration of the highest occupied molecular orbital (HOMO) energy and non-separated C-H and C=C peaks. Thus, the influences of the sizes, shapes, and types of edges of nanocarbon materials on the peak positions of C1s spectra have not been discussed in detail and are still unclear. (a) Characteristic structures of carbon materials (b) Conceptual image of this work.

Our recent work showed that the peak position of graphene-related materials with zigzag edges was higher than that with armchair edges and the peak position of graphene-related materials with zigzag edges was close to that of graphite (284.3 eV) [22]. A similar tendency was also observed in the presence of nitrogen in GNRs [23]. It indicates the possibility of distinguishing types of edges for GNRs by C1s XPS spectra. However, the study of XPS analysis of graphene-related materials with zigzag and armchair

edges without hetero atom demonstrated only calculated C1s XPS spectra [22], and not experimental ones except for tetracene, chrysene, and graphite. Besides, XPS spectra for graphene-related materials with edges other than zigzag and armchair edges and shapes other than rectangular shapes have not been investigated in the previous work [22]. Experimental peak positions and the consideration of edges and shapes are the most essential for analyzing various nanocarbon materials in the future.

In this work, effects of 1) molecular shapes of graphene-related materials, such as rectangular, triangle, hexagonal, and others, 2) molecular sizes of graphene-related materials, and 3) types of edges such as zigzag edges, which are similar to Solo, armchair edges, which are similar to Duo, Trio, Quartet/Quatro, and Quintet on peak positions of C1s XPS spectra were investigated in detail by combining experimental and calculated XPS analyses (Fig. 1b).

## Experimental

Graphite (HOPG, ZYH, NT-MDT Co.), graphite powder (SP270, Nippon Graphite Industries, Ltd.), and various aromatic compounds such as coronene (> 95.0%, TCI Co., Ltd.), pentacene (> 99%, Sigma-Aldrich Co. LLC.), hexabenzocoronene (> 95%, 1717 CheMall Corp.), dibenzo[b,def]chrysene (> 98.0%, TCI Co., Ltd.), perylene (> 99.5%, Sigma-Aldrich Co. LLC.), quaterrylene (purity not available, Sigma-Aldrich Co. LLC.), and triphenylene (> 98%, Sigma-Aldrich Co. LLC.) were analyzed experimentally using two XPS devices (AXIS ULTRA DLD

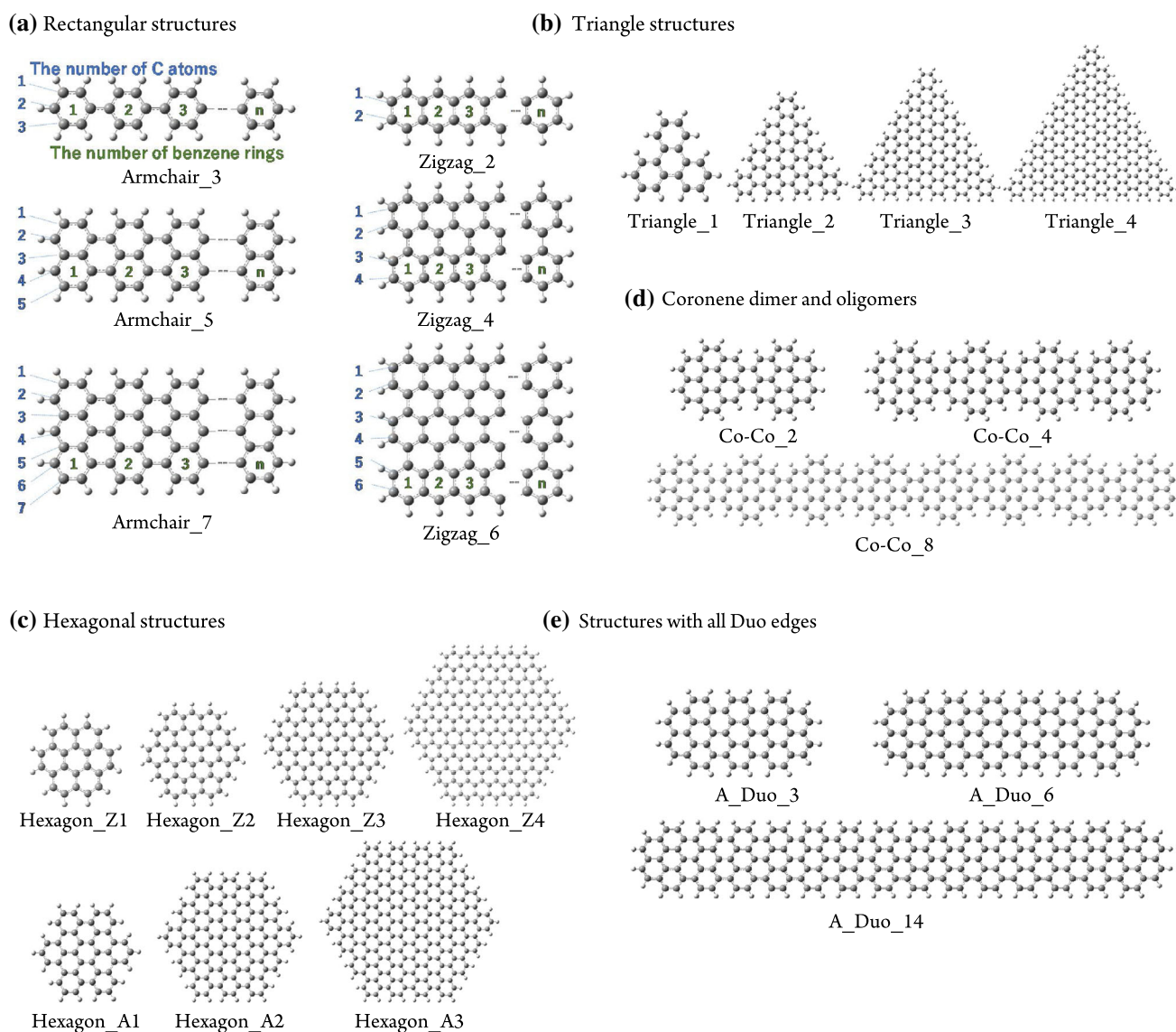
(Shimadzu Corp.) and JPS-9030 (JEOL Ltd.). The peak positions of C1s XPS spectra were adjusted by the shift of HOMO (Fig. S1). The influence of sizes of powder of analyzing samples on the peak positions and full width at half maximums (FWHMs) were also investigated. The detail is explained in Supplementary Material.

## Calculation

Six kinds of GNR-like rectangular structures (Fig. 2a), four triangle structures (Fig. 2b), and seven hexagonal structures with either zigzag or armchair edges

(Fig. 2c) were constructed as model structures for calculating XPS spectra. These structures were selected because graphene with different shapes such as rectangle [43–46], triangle [47, 48], and hexagonal structures [38–42] have been reported.

For the rectangular structures, benzene rings in the vertical direction were numbered from  $n = 3$  to 30 ( $n = 3, 6, 14,$  and  $30$  for zigzag-type structures and  $n = 3, 6, 14,$  and  $25$  for armchair-type structures), and carbon atoms in the horizontal direction were numbered from 3 to 7 for armchair edges and from 2 to 6 for zigzag edges (Fig. 2a). For example, Armchair\_3-3 represented the structure containing 3 benzene rings



**Figure 2** Modeled structures with different shapes. **a** Rectangular structures. **b** Triangle structures. **c** Hexagonal structures. **d** Coronene dimer and oligomers. **e** Structures with all Duo edges. (A color version of this figure can be viewed online).

**Table 1** The number of C and H atoms of structures, and the atomic ratio of H/C ( $n = \infty$ ) for structures as shown in Fig. 2

Name	The number of C atoms	The number of H atoms	The atomic ratio of H/C at $n = \infty$ (%)
Armchair_3	6n	4n + 2	67
Armchair_5	10n	4n + 4	40
Armchair_7	14n	4n + 6	29
Zigzag_2	4n + 2	2n + 4	50
Zigzag_4	8n + 4	2n + 8	25
Zigzag_6	12n + 6	2n + 12	17
Triangle	6n (2n + 1)	12n	0
Hexagon_Z	6n (n + 2) + 6	6n + 6	0
Hexagon_A	18n (n + 1) + 6	12n + 6	0
Co-Co	24n	8n + 4	33
A_Duo	14n + 10	4n + 8	29

arranged in the horizontal direction with armchair edges and 3 carbon atoms arranged in the vertical direction. As triangle structures, one structure with only Quartet (Triangle\_1) and three structures with Quartet and Duo (Triangle\_2, Triangle\_3, and Triangle\_4) were also constructed (Fig. 2b). As hexagonal structures, one structure with only Duo (Hexagon\_Z1), three structures with Solo and Duo (Hexagon\_Z2, Hexagon\_Z3, and Hexagon\_Z4), one structure with only Trio (Hexagon\_A1), and two structures with Duo and Trio (Hexagon\_A2 and Hexagon\_A3) were constructed (Fig. 2c). Structures of coronene dimer (Co-Co\_2) and oligomers (Co-Co\_4 and 8) with Solo and Duo (Fig. 2d) and structures with all Duo (A\_Duo\_3, A\_Duo\_6, and A\_Duo\_14) (Fig. 2e) were calculated. Both Co-Co\_1 and A\_Duo\_1 are coronene molecules, which are the same as Hexagon\_Z1. Structures not shown in Fig. 2 are also calculated, but the same definitions are applied to those structures.

The number of C and H atoms in structures and the atomic ratio of H/C ( $n = \infty$ ) for structures shown in Fig. 2 are summarized in Table 1. As the number of n becomes infinity, the atomic ratio of H/C of e.g., Armchair\_3 becomes 67%, whereas those of triangle and hexagonal structures become zero. In other words, the effects of the edges become negligible for triangle and hexagonal structures with large molecular weight because the atomic ratio of H/C becomes zero, whereas the effects of the edges (e.g., Duo for Armchair structures and Solo for Zigzag structures) become constant.

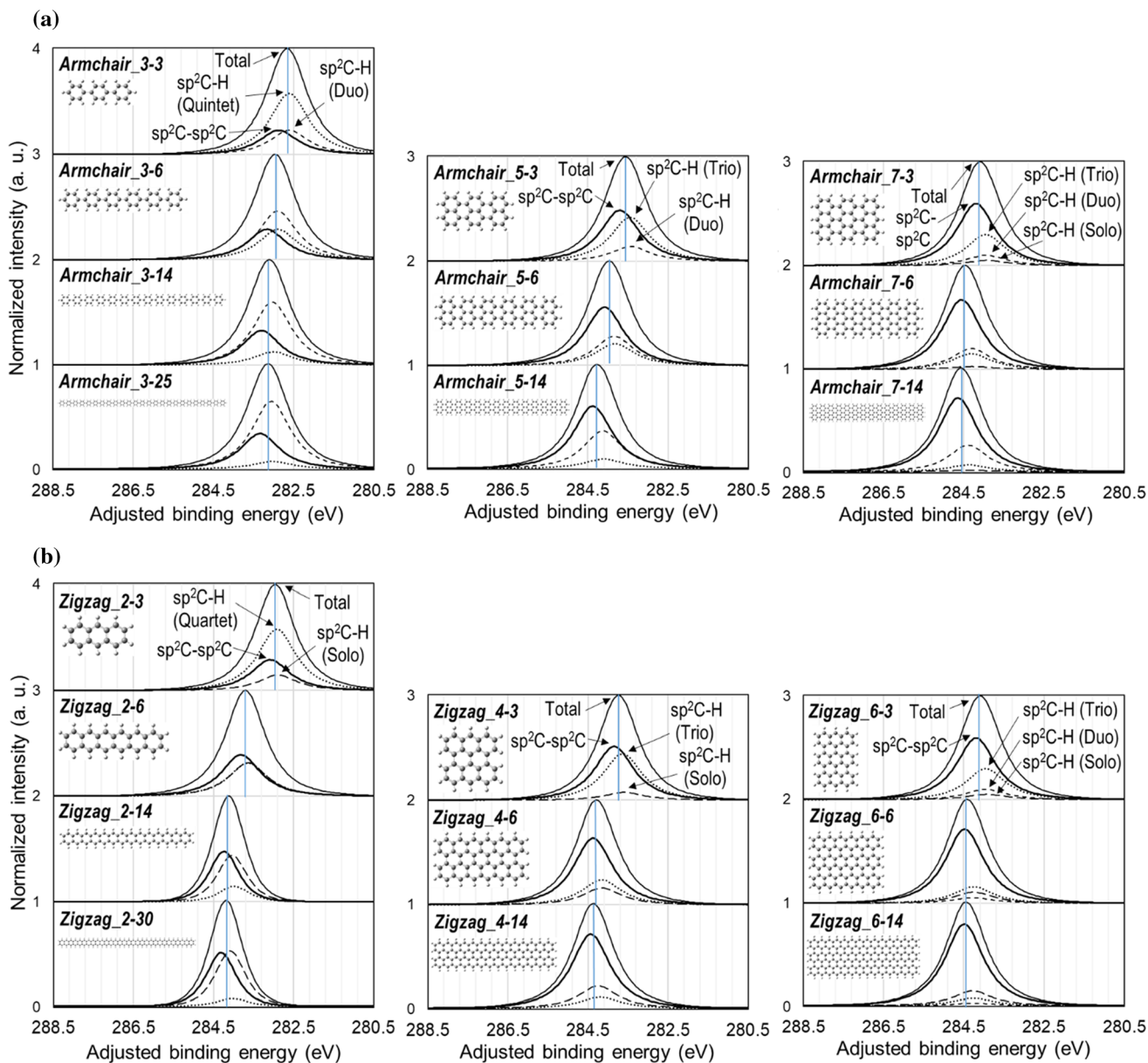
All of the calculations were conducted using B3LYP/6-31g(d) integral=grid=ultrafine of Gaussian

09 [90] in a similar way to our previous work [22, 63, 71–78, 82, 84–86] except for the introduction of symmetry to calculate structures with large molecular weight. For the rectangular structures, the triangle structures, the hexagonal structures, D2h, D3h, and D6h symmetries were applied, respectively. For structures of coronene and coronene dimer, and oligomers and structures with all Duo edges, D2h symmetry was applied. The symmetry was applied to calculate large molecules in this work because the accuracy of B3LYP/6-31g(d) is relatively high and the calculation of such large molecules using B3LYP/6-31g(d) without symmetry is difficult, although the other hybrid functionals are possible to be used without symmetry for large molecules [63]. The charge and spin multiplicity of the structures were set as 0 and 1. After the structures were optimized, orbital energies for simulated XPS spectra and Mulliken charges were calculated. For simulating C1s XPS spectra, the calculated orbital energies were used. The HOMO energy was subtracted from each orbital energy to calculate binding energies [22, 82, 84]. The calculated orbital energy was multiplied with 0.79282 and then 58.92 was further added to match the experimental and calculated binding energies (Table S1 and Figs. S2 and S3). Furthermore, modified asymmetric Voigt-type lineshape [91] was applied. The ratios of Lorentzian function to Gaussian function, m, and the asymmetry factor,  $\alpha$ , were 0.92 (Fig. S4) and 0, respectively, to compensate for the difference between the calculated and the experimental binding energies. The asymmetry factor ( $\alpha$ ) was set to 0 for easy comparison, although the experimental value was 0.22 for conductive materials

such as graphite (Fig. S4) [73]. Although the asymmetry factor and also the ratios of Lorentzian function to Gaussian function differ depending on the conductivity, the shapes of spectra are not discussed in this work in detail for ease of comparison. The detail of calculation and spectral shape is explained in Supplementary Material.

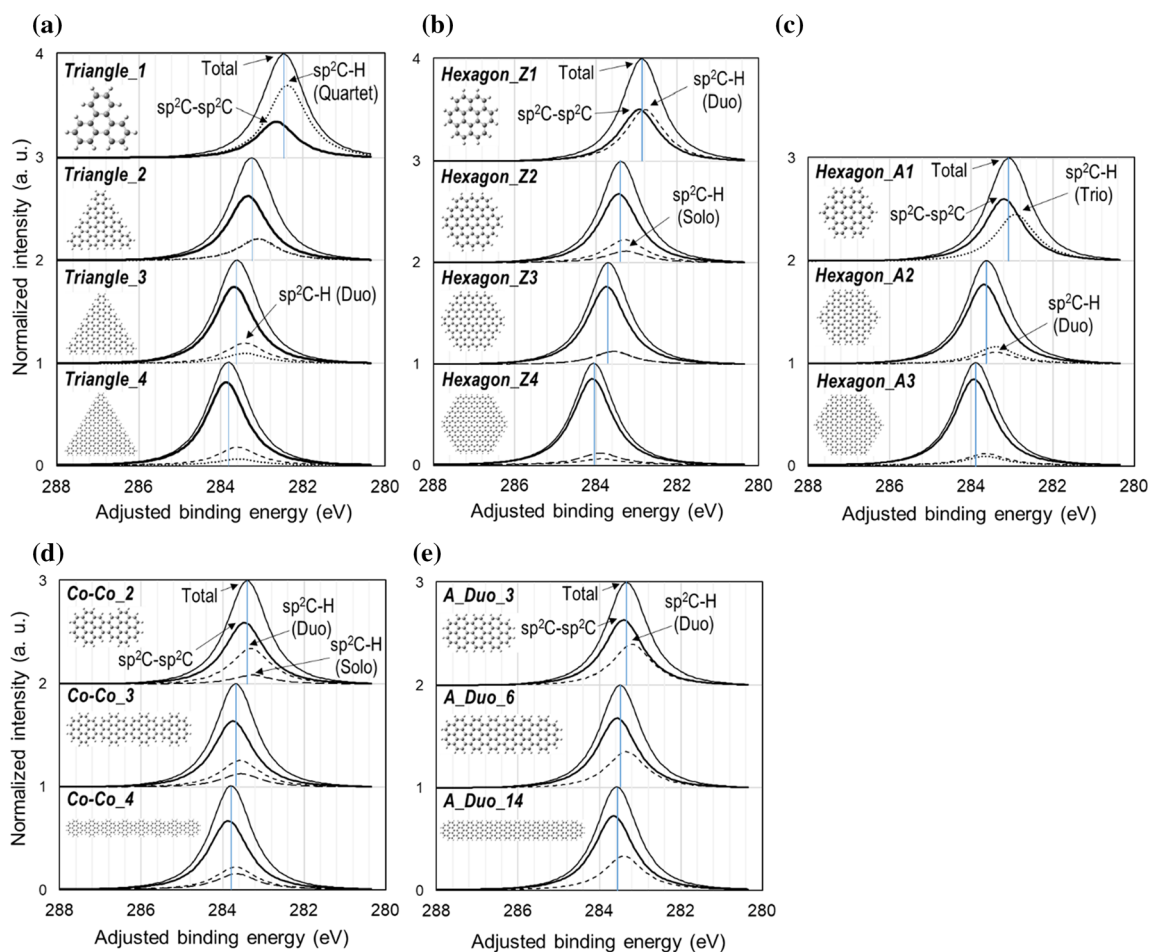
## Results and discussion

Figure 3 and Table S2 show simulated C1s XPS spectra of rectangular structures and the summarized peak positions, respectively. The differences in C1s peak tops among different types of structures with  $sp^2C-H$  are 0.1 eV or less. The differences in C1s peak



**Figure 3** Simulated C1s XPS spectra of rectangular structures. Simulated total spectra are shown as thin lines. Blue lines show the positions of the peak tops of C1s XPS spectra. Bold lines show the spectra of  $sp^2C-sp^2C$ , indicating carbon atoms bonded with carbon atoms.  $Sp^2C-H$  (Solo), (Duo), (Trio), (Quartet), and (Quintet) indicate carbon atoms bonded with hydrogen atoms at positions of Solo, Duo, Trio, Quartet, and Quintet, respectively.  $Sp^2C-H$  (Solo)

and (Duo) are shown as dashed and fine dashed lines, respectively.  $Sp^2C-H$  (Trio), (Quartet), and (Quintet) are shown as dotted lines. **a** Armchair\_3-*n*, Armchair\_5-*n*, and Armchair\_7-*n*, where the value of *n* is 3, 6, 14, or 25. **b** Zigzag\_2-*n*, Zigzag\_4-*n*, and Zigzag\_6-*n*, where the value of *n* is 3, 6, 14, or 30. (A color version of this figure can be viewed online.)



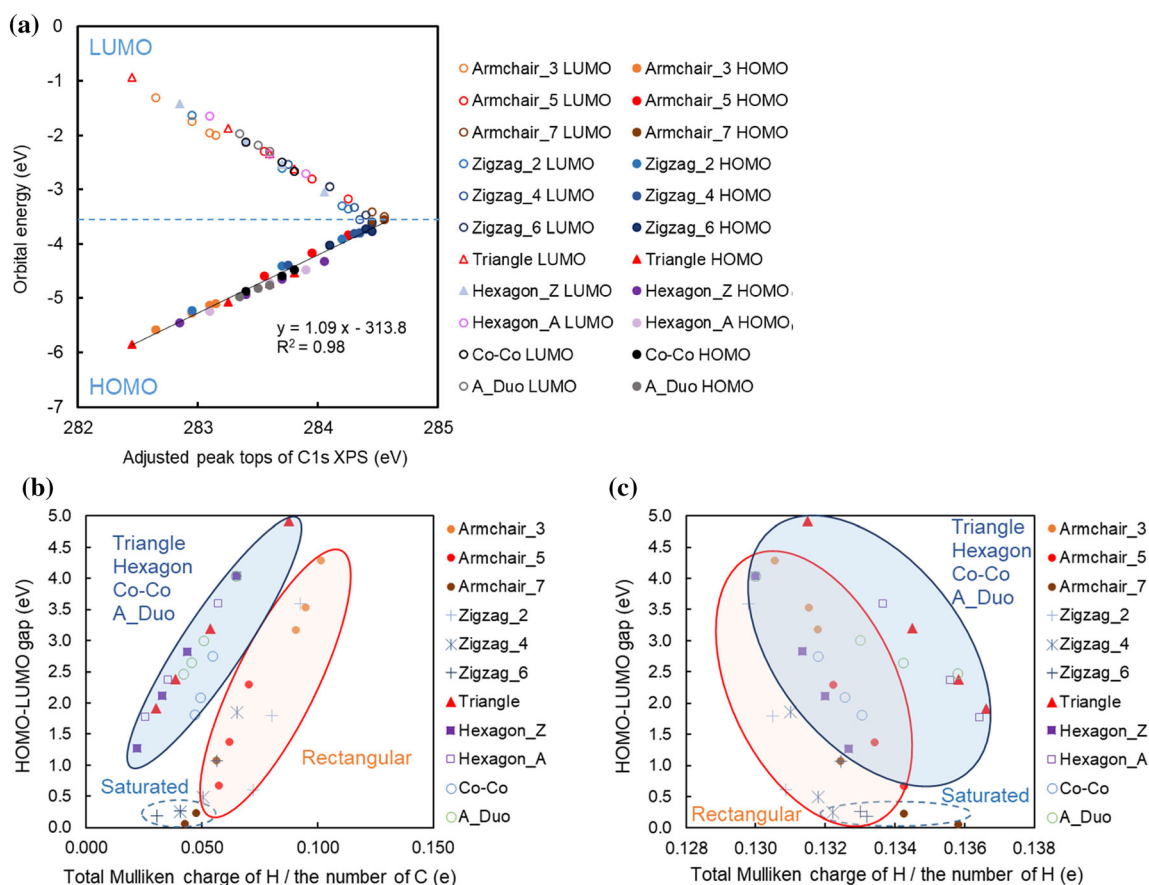
**Figure 4** Simulated C1s XPS spectra of triangle structures. Blue lines show the positions of the C1s peak tops. Simulated total spectra are shown as thin lines. Bold lines show the spectra of  $sp^2C-sp^2C$ , indicating carbon atoms bonded with carbon atoms.  $Sp^2C-H$  (Solo), (Duo), (Trio), and (Quartet) indicate carbon atoms bonded with hydrogen atoms at positions of Solo, Duo, Trio, and

Quartet, respectively.  $Sp^2C-H$  (Solo) and (Duo) are shown as dashed and fine dashed lines, respectively.  $Sp^2C-H$  (Trio) and (Quartet) are shown as dotted lines. **a** Triangle. **b** Hexagon\_Z. **c** Hexagon\_A. **d** Co-Co. **e** A\_Duo. (A color version of this figure can be viewed online.)

tops derived from  $sp^2C-sp^2C$  and  $sp^2C-H$  are 0.1–0.4 eV. The adjusted peak tops of C1s spectra shifted to higher binding energies as the  $n$  values of Armchair\_3- $n$ , Armchair\_5- $n$ , Armchair\_7- $n$ , Zigzag\_2- $n$ , Zigzag\_4- $n$ , and Zigzag\_6- $n$  increased. Besides, as the values of  $n$  increased, the peak shifts became smaller and became close to the peak position of graphite (284.3 eV in Fig. S2a and Table S1). Comparing the adjusted peak positions of C1s spectra of Zigzag and Armchair structures with comparable molecular sizes, the binding energies of Zigzag structures were higher than those of Armchair structures. This trend agrees with the trend of graphene-related materials with zigzag and armchair edges [22], which are different structures from the

structures used in this work. Unlike the previous work, we also calculated C1s XPS spectra of many graphene-related materials including other edges (Trio, Quartet, triangle, hexagonal, and the others) as explained below.

Figure 4 shows simulated C1s XPS spectra of triangle structures (Fig. 4a), hexagonal structures with zigzag (Fig. 4b) and armchair edges (Fig. 4c), coronene dimer and oligomers (Fig. 4d), and structures with all Duo edges (Fig. 4e). Table S2 shows the summary of the adjusted peak positions. The differences in C1s peak tops of  $sp^2C-H$  among Duo and Quartet, Solo and Duo, or Duo and Trio in different types of structures such as Hexagon\_Z2, Hexagon\_Z3, Hexagon\_A2, Hexagon\_A3, coronene



**Figure 5** Relation between adjusted peak tops of simulated C1s XPS spectra and the orbital energies of HOMO and LUMO. **a** Relation between the orbital energy of either HOMO or LUMO and adjusted peak tops of C1s XPS spectra. **b** Relation between the

HOMO–LUMO gap and the total Mulliken charge of H/ the number of C. **c** Relation between the HOMO–LUMO gap and the total Mulliken charge of H/ the number of H. (A color version of this figure can be viewed online).

dimer, and oligomers are 0.1 eV or less. Thus, it is challenging to separate the peaks corresponding to different types of edges in each structure. The differences in C1s peak tops derived from  $sp^2C$ - $sp^2C$  and  $sp^2C$ -H in each structure are 0.1–0.3 eV. As in the case of the rectangular structures shown in Fig. 3, the peak tops of C1s spectra for the triangle, hexagonal, and other structures shifted to higher binding energies as the  $n$  value of each structure increased. The degree of shifts became small as the value of  $n$  increased. Comparing the binding energies of C1s spectra of structures with equivalent molecular sizes in Fig. 4, the order was Hexagon\_Z > Hexagon\_A > Triangle, although the difference was small. The dependence of the shapes of graphene-like structures on the peak positions at various molecular weights is discussed later.

Comparing the adjusted peak positions of C1s spectra of structures with equivalent molecular sizes,

the peak positions of Co-Co 1 and A\_Duo 1, which are the same structure (coronene) as Hexagon\_Z1 (Fig. 4b), are close to the peak positions of Triangle\_1, and Hexagon\_A1, but the degrees of shifts to the high binding energy of Co-Co\_4 (Fig. 4d) and A\_Duo\_14 (Fig. 4e) were smaller than those of especially Hexagon\_Z and Hexagon\_A as the molecular weight increased because the gaps between HOMO and the lowest unoccupied molecular orbital (HOMO–LUMO) of Co-Co\_4 and A\_Duo\_14 were large even after the increment of the molecular weight, as explained later.

Figure 5 shows the relation between either HOMO or LUMO and the peak top of C1s spectra. For all of the structures (Figs. 2 and S6–S11), the relation between HOMO and the peak top of C1s spectra exhibited linear correlations (Fig. 5a), and the same tendency was obtained for LUMO. It indicates that the adjusted peak tops of C1s depend on the



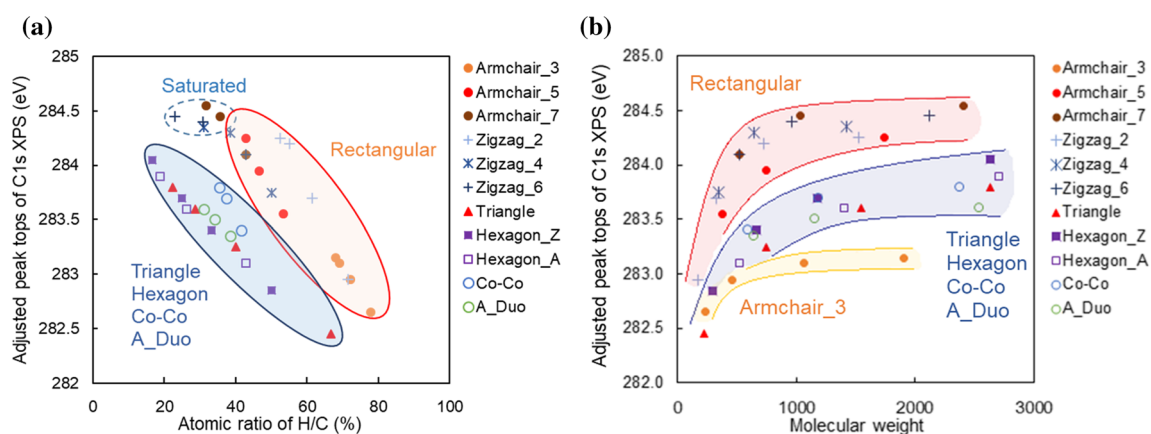
positions of HOMO. As the HOMO–LUMO gaps became smaller, C1s peak tops increased and reached ca. 284.5 eV, which was the upper limit of the peak tops of C1s spectra. Because HOMO directly influences the adjusted peak positions of C1s spectra, it is essential to investigate the dependence of shapes (Fig. 6a), molecular weight (Fig. 6b), and edge structures of carbon materials (Fig. 6ab) on the adjusted peak position of C1s spectra.

Figure 5b and c show the relation between the HOMO–LUMO gap and the total Mulliken charge of H/ the number of either C or H. The Mulliken charge was obtained from Figs. S6–S11 and summarized in Table S3 because of the possible trend depending on the types of edges. Negative Mulliken charge becomes higher from -0.37 to -0.12 in the order of carbon of Solo, Duo, Trio, Quartet, and Quintet, and the Mulliken charge approached -0.129 (carbon in benzene) from Solo to Quintet (Fig. S12). It is well known that carbon atoms on Solo become electrically rich as observed under scanning transmission electron microscopy [20] and calculated in our previous works [21]. Thus, obviously Solo is electronically rich but this work could obtain the order of Mulliken charge for all types of edges for hexagonal aromatic ring structures.

From Fig. 5b, it is obvious that two linear correlations, where the increment of “Mulliken charge of H/ the number of C” accompanies the increment of “the HOMO–LUMO gap”, were obtained depending on the shapes of graphene-like structures. Comparing at the same HOMO–LUMO gap, “the Mulliken charge of H/ the number of either C” of rectangular

structures was larger than those of triangle and hexagonal structures, indicating that carbon atoms in rectangular structures are electrically richer than triangle and hexagonal structures at the same number of carbon atoms.

In the basal plane of graphene-like structures (Figs. S6–S11), little increase or decrease in the number of electrons on carbon atoms was observed, and the Mulliken charges are about 0.00–0.02, which is equal to 6.00–6.02 electrons. In contrast, the change in the number of electrons on carbon atoms around the edges is large (Figs. S6–S11), affecting the electrons on the C atoms of C–Hs and the C atoms of the adjacent C=C bond to -0.37–0.25 (= 5.63–6.25 electrons). The number of electrons in the H of the C–H at the edge also tends to increase, meaning that Mulliken charge of hydrogen decreases, as the GNR widens or lengthens, but the increase is slight, and in some structures, there is almost no increase. For example, the Mulliken charge of H on DUO in the center of structures increases from 0.131 to 0.135 as the width increases from Armchair\_3-3 to Armchair\_7-3, but there is almost no change from 0.129 to 0.130 for Zigzag structures as the width increases from Zigzag\_2-3 to Zigzag\_6-3 (Fig. S7). Because rectangular structures contain more carbon atoms close to edges than the other structures, the Mulliken charge of hydrogen per carbon is larger for rectangular structures (Fig. 5b). Therefore, the differences observed in Fig. 5bc due to the different shapes and in Fig. 6ab, which will be discussed later, are mainly due to the larger proportion of C atoms adjacent to the edges or edges affected by the C–H on edges. However, this



**Figure 6** Relation between adjusted peak tops of C1s XPS spectra and either the atomic ratio of H/C or the molecular weight. **a** Relation between the percentage of atomic ratios of H/C and

adjusted peak tops of C1s spectra. **b** Relation between molecular weight and peak tops of total C1s spectra. (A color version of this figure can be viewed online).

alone does not explain the difference between Armchair structures and Co-Co/A\_Duo structures, because Co-Co and A\_Duo structures also contain many edges.

There are two main differences among armchair, Co-Co, and A\_Duo structures. The first difference is the presence of zigzag edges at both ends of the GNRs for armchair structures (Table 2) and the presence of zigzag-like edges [57] for Co-Co structures (Table 3). In Co-Co and A\_Duo, the HOMO–LUMO gap is wider due to the absence of zigzag edges at both ends, and the trend is different from armchair structures as shown in HOMO orbitals in Tables 2 and 3. By comparing zigzag-like edges on Co-Co structures and armchair edges on A\_Duo, HOMO–LUMO gaps of Co-Co structures with zigzag-like edges were smaller than those of armchair edges on A\_Duo. The second difference is the ease of conjugation. As the aromatic ring increases, C=C on DUO tends to be more doubly bonded than 1.5-bonded according to Clar's law [92]. As C=C on Duo becomes short, being close to double bond, C–C bond between one of the Cs on Duo and the C bonded to the C on Duo becomes long, resulting in possible less conjugation.

In fact, as shown in Fig. 7a, in Armchair\_3, where the benzene rings are bonded to each other to form linear chain structures, even though the molecular weight of Armchair\_3 becomes larger (up to 1904), the length of C=C on Duo is almost the same and approximately 1.39 Å. In contrast, the lengths of C=C on Duo in the structures of Co-Co and A\_Duo are also the same but much shorter (1.37 Å) (Fig. 7a). As shown in Fig. 7c, the length of the C=C bond on Duo in the structure of Armchair\_3-3 drawn by GaussView's software is approximately 1.39 Å and the C=C bond is drawn as 1.5 bond rather than a double bond, whereas that of the C=C bond on Duo in the structure of A\_Duo\_3 is as short as 1.37 Å and the C=C bond is drawn as double bond. From the above and other results, it was found that the lengths of C=C on Duo are particularly long in the Armchair structures, while those in other structures (Co-Co, A\_Duo, Triangle, and Hexagon\_A) are short. The relation between the length of bonding and binding energy of N1s orbital has been reported [93]. Therefore, the bond length of C=C is also considered to be one of the important factors for the shift of C1s XPS spectra.

In addition to the change in the length of C=C on Duo, the bond length between the C on Duo and C





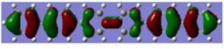




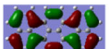
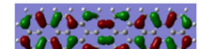
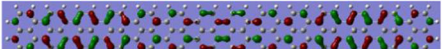
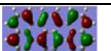
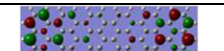

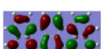

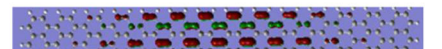


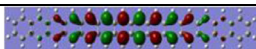


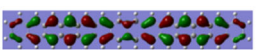
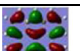

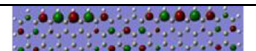
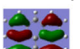

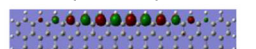
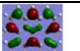
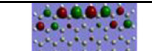
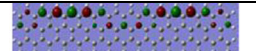
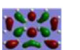
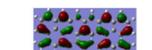

next to Duo is also crucial (Fig. 7bc). The long bond length between C on Duo and C next to Duo and the shortening of C=C on Duo probably cause the part of Duo to be less related to conjugation, resulting in a wider band gap. In addition, a steric hindrance is present between two C-Hs on Duo [59, 60], and this steric hindrance may also have affected the C=C length explained above, but in the case of the same Armchair with different lengths in width (especially the less rotatable Armchair\_5 and Armchair\_7), the difference is difficult to explain by the steric hindrance. Thus, the difference is considered to come from the change in the conjugate state. These changes in the length of Duo and C=C surrounding Duo are important not only in the XPS discussion but also in other studies because they affect the peak positions of D' band, which is related to the quadrant stretching vibration of C=C derived from the defect structure in Raman and IR spectroscopic analysis [94].

In the triangle and hexagonal structures, the Solo edge is prevented from extending longer by the presence of Quartet, Trio, and Duo. Thus, the electrons on carbon atoms in the Solo in triangle and hexagonal structures are less likely to be conjugated than rectangular structures with zigzag edges even when the molecular weight increases, and the triangle and hexagonal structures are expected to have wider band gaps than Armchair\_Z.

Comparing the lengths of C=Cs on Duo in Fig. 7ab with those between C on Solo and C next to Solo (Fig. 8a) as well as those of C=C next to Solo (Fig. 8b), it is found that the lengths of C=C between C on Solo and C next to Solo (Fig. 8a) as well as the C=C next to Solo (Fig. 8b) are longer than those of the C=C of Duo (Fig. 7a) and the C=C between the carbon atom on Duo and the neighboring bonded carbon atom (Fig. 7b), respectively. In Zigzag\_2 (Fig. 8b), as the molecular weight increases, the C=C next to Solo becomes much longer, much closer to the single bond, which makes it easier to conjugate at Solo and the next C on the edges of GNRs, resulting in a narrower HOMO–LUMO gap even at small molecular weights. Although not directly related to this XPS study, the longer C=C next to Solo correlates with the smaller force constant in Raman and IR analyses [95], which leads to a lower shift in the G band for GNR with zigzag edges, although it has not been explained in our previous work [22].

Figure 5c shows that as “the Mulliken charge of H/ the number of H” increases, “the HOMO–LUMO

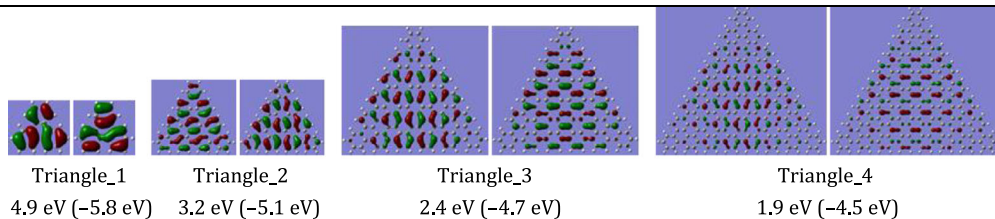
**Table 2** HOMO and NHOMO of rectangular structures. **a** Armchair edges. **b** Zigzag edges. The numbers without parentheses are HOMO–LUMO gaps, and the numbers in parentheses are orbital energies of HOMO. (A color version of this table can be viewed online.)

<b>(a) Armchair edges</b>			
HOMO			
	Armchair_3-3 4.3 eV (–5.6 eV)	Armchair_3-6 3.5 eV (–5.3 eV)	Armchair_3-14 3.2 eV (–5.1 eV)
NHOMO			
	(–6.7 eV)	(–5.8 eV)	(–5.3 eV)
HOMO			
	Armchair_5-3 2.3 eV (–4.6 eV)	Armchair_5-6 1.4 eV (–4.2 eV)	Armchair_5-14 0.7 eV (–3.8 eV)
NHOMO			
	(–6.0 eV)	(–5.0 eV)	(–4.2 eV)
HOMO			
	Armchair_7-3 1.1 eV (–4.0 eV)	Armchair_7-6 0.2 eV (–3.6 eV)	Armchair_7-14 0.1 eV (–3.6 eV)
NHOMO			
	(–5.6 eV)	(–5.0 eV)	(–4.8 eV)
<b>(b) Zigzag edges</b>			
HOMO			
	Zigzag_2-3 3.6 eV (–5.2 eV)	Zigzag_2-6 1.8 eV (–4.4 eV)	Zigzag_2-14 0.6 eV (–3.9 eV)
NHOMO			
	(–6.5 eV)	(–5.5 eV)	(–4.3 eV)
HOMO			
	Zigzag_4-3 1.9 eV (–4.4 eV)	Zigzag_4-6 0.5 eV (–3.8 eV)	Zigzag_4-14 0.3 eV (–3.80 eV)
NHOMO			
	(–6.1 eV)	(–4.7 eV)	(–3.81 eV)
HOMO			
	Zigzag_6-3 1.1 eV (–4.0 eV)	Zigzag_6-6 0.3 eV (–3.7 eV)	Zigzag_6-14 0.2 eV (–3.77 eV)
NHOMO			
	(–5.6 eV)	(–4.3 eV)	(–3.81 eV)

**Table 3** HOMO and NHOMO of triangle, hexagonal, and the other structures. **a** Triangle structures. **b** Hexagonal structures. **c** The other structures. The numbers without parentheses are the HOMO–LUMO gaps, and the numbers in parentheses are the orbital energies of

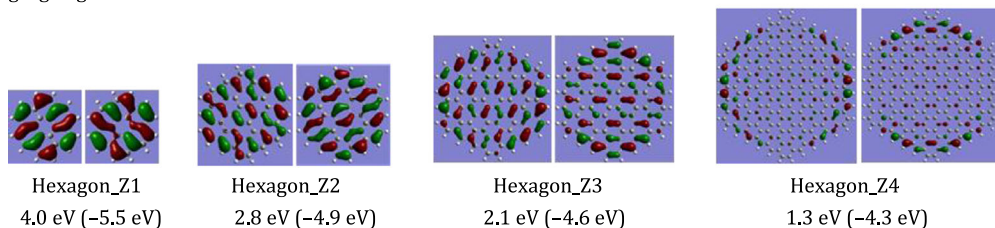
HOMO. In case that two structures are shown and only one energy is listed, the HOMO and NHOMO have the same energy. For two similar structures in this table, the left side is HOMO and the right side is the NHOMO. (A color version of this table can be viewed online.)

**(a) Triangle structures**

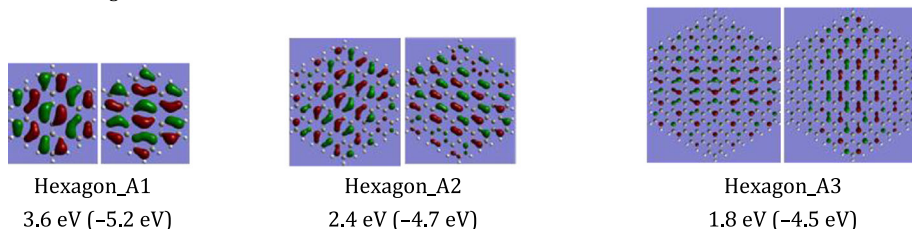


**(b) Hexagonal structures**

i) With zigzag edges

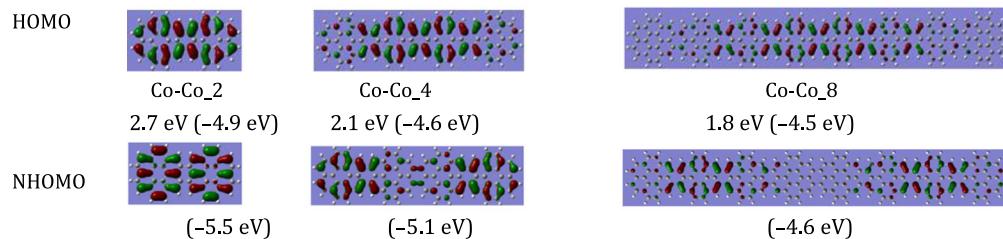


ii) With armchair edges

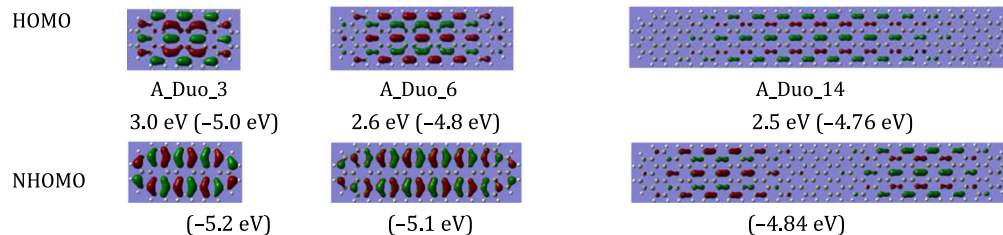


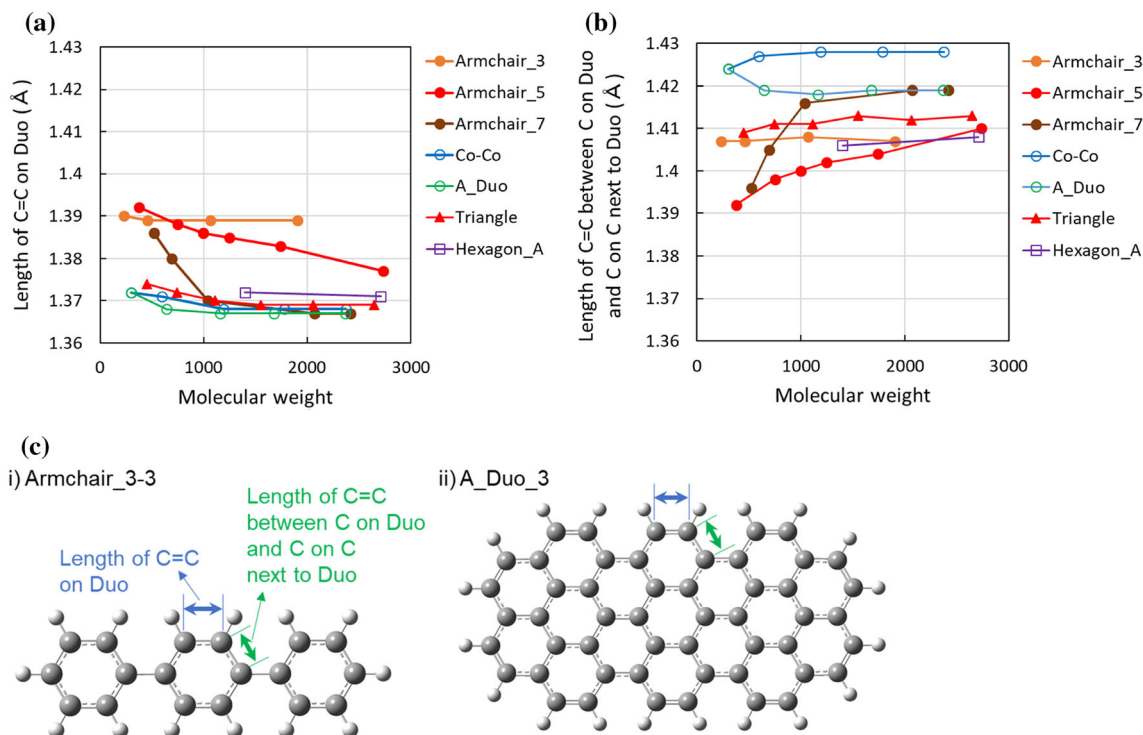
**(c) Others**

i) Co-Co



ii) A\_Duo





**Figure 7** Bond lengths of C=Cs either **a** on Duo or **b** between C on Duo and C next to Duo and **c** the examples of the bond length analyzed in **a** and **b**. The bond lengths of C=Cs were obtained from

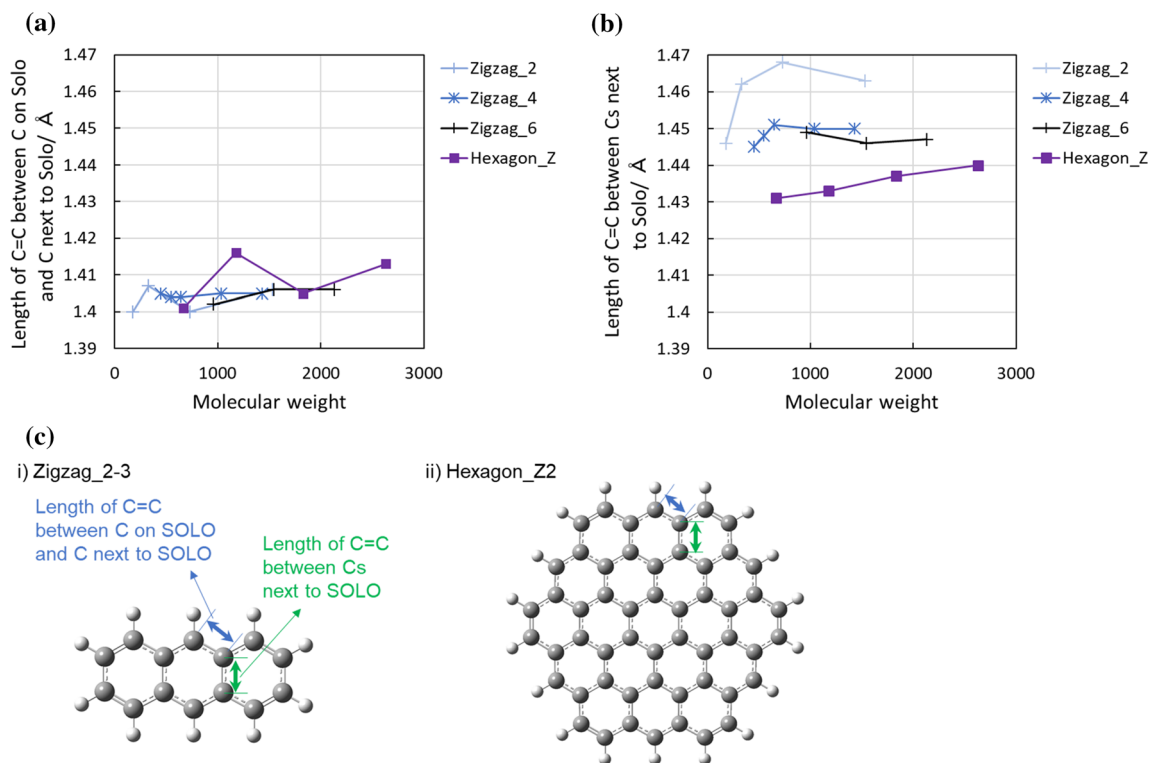
edges in the middle of each structure. (A color version of this figure can be viewed online).

gap” decreases, which is the opposite trend of Fig. 5b. As the molecular weight becomes large, the averaged Mulliken charge on hydrogen, which is written as “total Mulliken charge on hydrogen/ the number of hydrogen”, increased (Figs. 5c and S6-S11). The HOMO–LUMO gaps of Triangle and Hexagon\_A structures were larger than those of the rectangular structures at the same “Total Mulliken charge of H/ the number of H”, while those of Hexagon\_Z and Co-Co were similar to those of rectangular structures. Among rectangular structures, the HOMO–LUMO gaps of structures with zigzag edges are smaller than those of structures with armchair edges at the same “Total Mulliken charge of H/ the number of H”. In a similar way to Zigzag structures, the plots of Hexagon\_Z were positioned in the area of rectangular structures, probably because zigzag edges in Hexagon\_Z tend to lower the HOMO–LUMO gap. Because of the higher correlation of Fig. 5b than c, Fig. 5b can be utilized to analyze the shapes of graphene-related materials.

Figure 6 shows the dependence of shapes (Fig. 6a), molecular weight (Fig. 6b), and the edge structures of graphene-like materials (Fig. 6ab) on the

adjusted peak tops of C1s spectra. The percentage of atomic ratios of H/C and adjusted peak tops of C1s spectra showed a high linear correlation except for some structures that reached the maximum peak position of C1s spectra and saturated at ca. 284.5 eV (Fig. 6a).

Interestingly, rectangular structures showed a different trend from the other structures such as triangle, hexagonal, Co-Co, and A\_Duo structures in Fig. 6ab. It is mainly because the HOMO–LUMO gaps of rectangular structures tend to become much smaller than those of the other structures (Fig. 5a). Thus, the adjusted peak positions of C1s spectra of rectangular structures such as GNRs tended to be higher than those of the other structures at the same atomic ratio of H/C (Fig. 6a). One of the reasons is that rectangular structures of GNRs enhanced conjugation. At less than 40% of the percentage of the atomic ratio of H/C, peak tops of C1s spectra of Armchair\_7, Zigzag\_4 and Zigzag\_6 saturated at 284.3–284.5 eV. The orbital energies of HOMO of the corresponding structures saturated with the values at -3.8 eV– -3.6 eV, whose values depend on structures, and HOMO–LUMO gaps were 0.3 eV or less



**Figure 8** Bond length of C=C either **a** between C on Solo and C next to Solo or **b** between Cs next to Solo and **c** the examples of the bond length analyzed in **a** and **b**. The bond lengths of C=Cs

were obtained from edges in the middle of each structure. (A color version of this figure can be viewed online).

(Fig. 5a). Thus, peak tops of C1s saturate, as the atomic ratios of H/C become smaller (Fig. 6a) and the molecular weights become larger (Fig. 6b). As the widths of armchair and zigzag GNRs increase, peak tops of C1s spectra shifted higher (HOMO energy becomes higher and HOMO–LUMO gap becomes smaller (Fig. 5)). The tendency is consistent with the well-known reported electronic states [24, 96]. From the results explained above, this work could show the correlation between electronic states and C1s XPS spectra.

For all structures, adjusted peak tops of C1s spectra increase with the increment of molecular weight (Fig. 6b). As the molecular weight becomes large, the atomic ratios of H/C become constants (Table 1) and the orbital energies of HOMO and the peak positions of C1s become unchanged (Table S2). HOMO energies of rectangular structures tend to approach the Fermi level at a relatively small molecular weight (ca. 1,000), reaching the peak position of C1s XPS spectrum to the binding energy of graphite (284.3 eV) or even higher. The experimental binding energy for graphite is 284.3 eV (Table S1), but in Figs. 5a and 6b,

the maximum value of the peak positions exceeds 284.3 eV. This is because the HOMO of graphene-like structures used to calculate the scaling factor is farther from the Fermi level than those of structures that exceed 284.3 eV.

Unlike other rectangular structures, Armchair\_3 saturated the adjusted peak top of C1s spectra at 283.1 eV (Fig. 6b). One of the reasons is the lower limit of the atomic ratio of H/C for Armchair\_3 (Table 1), causing a large HOMO–LUMO gap (Table S2). However, the adjusted peak positions of C1s spectra for triangle and the hexagonal structures increased without saturation up to the molecular weight of ca. 2,700 (2,640 for Triangle\_4, 2,630 for Hexagon\_Z4, and 2,706 for Hexagon\_A3). It is expected that the adjusted peak tops of triangle and hexagonal structures keep increasing up to the peak position of graphite because triangle and hexagonal structures reach graphene as the molecular weight increases (Table 1).

Using the relation in Fig. 6a, the shape of the graphene-related materials can be estimated by measuring the sample using combustion elemental

analysis and XPS. For example, the H/C can be obtained from the experimental measurement of combustion elemental analysis, and the peak positions of C1s spectra and the HOMO positions can be determined from the experimental measurement of XPS (Fig. S1 and S2). Thus, it is possible to distinguish the structures among rectangular and triangle/hexagonal. Besides, if the molecular shape is known and the peak positions of C1s and HOMO can be obtained by calculation, the molecular weight can be estimated from Fig. 6b. For example, if the molecular shape is Zigzag\_2 and the peak top of measured C1s XPS spectra is 283.2 eV, which is not plotted in Fig. 6, the molecular weight is estimated to be 228 (C<sub>18</sub>H<sub>12</sub>). Thus, the structure is presumed to be Zigzag\_2-4. Using Fig. 6b, the molecular shape can be narrowed down to some extent among various molecular shapes by obtaining the molecular weight experimentally from the mass spectrometry and the experimental peak positions of C1s spectra and HOMO. In other words, by utilizing combustion elemental analysis, mass spectrometry, C1s, and HOMO, it is possible to estimate the structure of graphene-related materials.

Table 2 shows HOMO and the next HOMO (NHOMO) of rectangular structures with either armchair (Table 2a) or zigzag edges (Table 2b). Electron densities of HOMO reveal a more detailed relationship between the shape/types of edges/the molecular sizes and the orbital energy of HOMO, which directly relates to adjusted peak positions of C1s spectra. By increasing the width of armchair structures, zigzag edges appeared on both sides of Armchair\_7 and the zigzag edges became HOMO of Armchair\_7-6 and 7-14. It has been reported that carbon atoms on zigzag edges become electrically rich as observed under scanning transmission electron microscopy [20] and calculated in our previous works [21]. Rectangular structures with zigzag edges have higher conjugation at the HOMO level than those with armchair edges, generating conductive path on zigzag edges and causing a smaller HOMO–LUMO gap.

Table 3 shows HOMO and NHOMO of triangle, hexagonal, and other structures. For triangle structures in Table 3a and hexagonal structures in Table 3b, both HOMO and NHOMO are shown because the two orbital energies were close to each other, whereas the energies of HOMO and NHOMO of other structures are a little far from each other

(Tables 2 and 3). As the molecular weight of hexagonal structures becomes large (Table 3b), HOMO for Hexagon\_Z are localized on zigzag edges, while those for Hexagon\_A are delocalized in the basal plane as for triangle structures (Table 3a) because both Hexagon\_A and triangle structures contain armchair edges. A similar tendency was observed in previous work [97]. Armchair\_7 (Table 2a), Co-Co (Table 3ci), and A\_Duo (Table 3cii) have the same width except for the concaved shape of Co-Co and A\_Duo. The peak positions of C1s spectra for Co-Co are closer to those for A\_Duo than those for Armchair\_7 (Fig. 6b and Table S2). As the molecular size of Co-Co and A\_Duo became larger, HOMOs were localized in the middle of the molecule (Table 3) because Co-Co and A\_Duo contain no zigzag edges on both sides, unlike Armchair\_7.

Using the results of this work, peak tops of C1s spectra of graphene-related materials can be predicted from the molecular shape and molecular size, if the molecular structures of graphene-related materials had regularity. The molecular shape and molecular size can also be estimated from experimental peak tops of C1s spectra if molecular structures of the graphene-related materials had regularity. Especially, by combining this technique with other techniques such as infrared spectroscopy [57] and Raman spectroscopy [22], the estimation of structures becomes much more reliable. However, it has to keep in mind that the peak position of carbon materials with low molecular weight may be influenced by the sizes of power of analyzed samples due to a charge-up effect (Fig. S13). Samples in the form of fine powder tend to show the smaller FWHM (Fig. S13c) and the lower peak position (Fig. S13ab) than those of coarse powder. The spectral shapes are also influenced by the analytical conditions such as pass energy (Fig. S14) and the conductivity of samples [82]. Therefore, the appropriate analysis conditions have to be applied in order to utilize the method in this work.

## Conclusions

The influence of shapes and molecular weight of graphene-like structures on adjusted peak positions of C1s XPS spectra was investigated by calculating C1s XPS spectroscopy in addition to the experimental C1s XPS spectra of the model compounds with

various edge structures and we suggested the estimation methods of molecular structures of graphene-related materials from C1s XPS spectra. This work revealed that the adjusted peak positions of C1s XPS spectra of rectangular structures such as GNRs tended to be higher than those of triangle, hexagonal, and the other structures at the same atomic ratio of H/C mainly because rectangular structures of GNRs enhanced the conjugation more than those of hexagonal and triangle structures of graphene-related materials and HOMO becomes close to Fermi level. Besides, as the molecular weight increased, the HOMO energy approached the Fermi level, causing the shift of the adjusted peak position of the C1s XPS spectrum of graphene-related materials close to that of graphene, although some structures showed much low binding energy of C1s spectra even though the molecular weight increased. Since H/C, molecular weight, and the difference between C1s XPS and HOMO can be experimentally obtained by combustion elemental analysis, mass spectrometry, and XPS, the relationship obtained in this work between the adjusted peak position of C1s XPS spectra and either the H/C ratio or molecular weight can be utilized to estimate the shapes and types of edges of graphene-related materials.

## Acknowledgements

This work was supported by JSPS KAKENHI Grant Number JP21K04773.

## Declarations

**Conflict of interest** Conflict of interest the authors declare that they do not have any conflict of interest

**Supplementary Information:** The online version contains supplementary material available at <http://doi.org/10.1007/s10853-022-07599-6>.

## References

- [1] Geim AK, Novoselov KS (2017) The rise of graphene. *Nat Mater* 6:183–191
- [2] Radushkevich LV, Lukyanovich VM (1952) The structure of carbon forming in thermal decomposition of carbon monoxide on an iron catalyst. *Sov J Phys Chem* 26:88–95
- [3] Ijima S, Ichihashi T (1993) Single-shell carbon nanotubes of 1-nm diameter. *Nature* 363:603–605
- [4] Yang X, Dou X, Rouhanipour A, Zhi L, Räder HJ, Müllen K (2008) Two-dimensional graphene nanoribbons. *J Am Chem Soc* 130:4216–4217
- [5] Choi W, Lahiri I, Seelaboyina R, Kang YS (2010) Synthesis of graphene and its applications: a review. *Crit Rev Solid State Mater Sci* 35:52–71
- [6] Agudosi ES, Abdullah EC, Numan A, Mubarak NM, Khalid M, Omar N (2020) A review of the graphene synthesis routes and its applications in electrochemical energy storage. *Crit Rev Solid State Mater Sci* 45:339–377
- [7] Zhang Y, Heo YJ, Son YR, In I, An KH, Kim BJ, Park SJ (2019) Recent advanced thermal interfacial materials: a review of conducting mechanisms and parameters of carbon materials. *Carbon* 142:445–460
- [8] González M, Pozuelo J, Baselga J (2018) Electromagnetic shielding materials in GHz range. *Chem Rec* 18:1000–1009
- [9] Wu N, Hu Q, Wei R, Mai X, Naik N, Pan D, Guo Z, Shi Z (2021) Review on the electromagnetic interference shielding properties of carbon based materials and their novel composites: Recent progress, challenges and prospects. *Carbon* 176:88–105
- [10] Li X, Yu J, Wageh S, Al-Ghamdi AA, Xie J (2016) Graphene in photocatalysis: a review. *Small* 12:6640–6696
- [11] Amollo TA, Mola GT, Kirui MSK, Nyamori VO (2018) Graphene for thermoelectric applications: prospects and challenges. *Crit Rev Solid State Mater Sci* 43:133–157
- [12] Julkapli NM, Bagheri S (2015) Graphene supported heterogeneous catalysts: An overview. *Int J Hydrog Energy* 40:948–979
- [13] Mohan VB, Lau K, Hui D, Bhattacharyya D (2018) Graphene-based materials and their composites: a review on production, applications and product limitations. *Compos B: Eng* 142:200–220
- [14] Tao L, Wang Q, Dou S, Ma Z, Huo J, Wang S, Dai L (2016) Edge-rich and dopant-free graphene as a highly efficient metal-free electrocatalyst for the oxygen reduction reaction. *Chem Commun* 52:2764–2767
- [15] Ikeda T, Hou Z, Chai GL, Terakura K (2014) Possible oxygen reduction reactions for graphene edges from first principles. *J Phys Chem C* 118:17616–17625
- [16] Pak AJ, Paek E, Hwang GS (2014) Impact of graphene edges on enhancing the performance of electrochemical double layer capacitors. *J Phys Chem C* 118:21770–21777
- [17] Zhan C, Zhang Y, Cummings PT, Jiang D (2017) Computational insight into the capacitive performance of graphene edge planes. *Carbon* 116:278–285



- [18] Afshari F, Ghaffarian M (2017) Electronic properties of zigzag and armchair graphene nanoribbons in the external electric and magnetic fields. *Physica E* 89:86–92
- [19] Kobayashi Y, Fukui K, Enoki T, Kusakabe K, Kaburagi Y (2005) Observation of zigzag and armchair edges of graphite using scanning tunneling microscopy and spectroscopy. *Phys Rev B* 71:193406
- [20] Kobayashi Y, Fukui K, Enoki T, Kusakabe K (2006) Edge state on hydrogen-terminated graphite edges investigated by scanning tunneling microscopy. *Phys Rev B* 73:125415
- [21] Yamada Y, Kawai M, Yorimitsu H, Otsuka S, Takanashi M, Sato S (2018) Carbon materials with zigzag and armchair edges. *ACS Appl Mater Interfaces* 10:40710–40739
- [22] Kim J, Lee N, Min YH, Noh S, Kim N, Jung S, Joo M, Yamada Y (2018) Distinguishing zigzag and armchair edges on graphene nanoribbons by X-ray photoelectron and Raman spectroscopies. *ACS Omega* 3:17789–17796
- [23] Yamada Y, Tanaka H, Kubo S, Sato S (2021) Unveiling bonding states and roles of edges in nitrogen-doped graphene nanoribbon by X-ray photoelectron spectroscopy. *Carbon* 185:342–367
- [24] Barone V, Hod O, Scuseria GE (2006) Electronic structure and stability of semiconducting graphene nanoribbons. *Nano Lett* 6:2748–2754
- [25] Yamaguchi J, Hayashi H, Jippo H, Shiotari A, Ohtomo M, Sakakura M, Hieda N, Aratani N, Ohfuchi M, Sugimoto Y, Yamada H, Sato S (2020) Small bandgap in atomically precise 17-atom-wide armchair-edged graphene nanoribbons. *Commun Mater* 1:36
- [26] Stein SE, Brown RL (1987)  $\pi$ -Electron properties of large condensed polyaromatic hydrocarbons. *J Am Chem Soc* 109:3721–3729
- [27] Yano Y, Mitoma N, Ito H, Itami K (2020) A quest for structurally uniform graphene nanoribbons: synthesis, properties, and applications. *J Org Chem* 85:4–33
- [28] Geoenewege MP (1956) Some regularities in the infra-red spectra of polynuclear aromatic compounds in the C-H wagging region. *Spectrochim Acta* 11:579–575
- [29] Aihara J (1987) Photochemical stability of polycyclic aromatic hydrocarbons in the interstellar medium. *Bull Chem Soc Jpn* 60:3143–3147
- [30] Hony S, Kerckhoven C, Peeters E, Tielens AGGM, Hudgins DM, Allamandola LJ (2001) The CH out-of-plane bending modes of PAH molecules in astrophysical environments. *Astron Astrophys* 370:1030–1043
- [31] Hu A, Duley WW (2008) Surface enhanced Raman spectroscopic characterization of molecular structures in diamond-like carbon films. *Chem Phys Lett* 450:375–378
- [32] Sadjadi S, Zhang Y, Kwok S (2015) On the origin of the 11.3 micron unidentified infrared emission feature. *Astrophys J* 807(1):95
- [33] Pauzat F, Talbi D, Ellinger Y (1997) The PAH hypothesis: a computational experiment on the combined effects of ionization and dehydrogenation on the IR signatures. *Astron Astrophys* 319:318–330
- [34] Centrone A, Brambilla L, Renouard T, Gherghel L, Mathis C, Müllen K, Zerbi G (2005) Structure of new carbonaceous materials: The role of vibrational spectroscopy. *Carbon* 43:1593–1609
- [35] Bauschlicher CW Jr, Peeters E, Allamandola LJ (2009) The infrared spectra of very large irregular polycyclic aromatic hydrocarbons (PAHs): observational probes of astronomical PAH geometry, size and charge. *Astrophys J* 697:311–327
- [36] Tommasini M, Lucotti A, Alfè M, Ciajolo A, Zerbi G (2016) Fingerprints of polycyclic aromatic hydrocarbons (PAHs) in infrared absorption spectroscopy. *Spectrochim Acta A* 152:134–148
- [37] Chang Q, Gao R, Li H, Yu G, Wang F (2018) Effect of CO<sub>2</sub> on the characteristics of soot derived from coal rapid pyrolysis. *Combust Flame* 197:328–339
- [38] Wu B, Geng D, Guo Y, Huang L, Xue Y, Zheng J, Chen J, Yu G, Liu Y, Jiang L, Hu W (2011) Equiangular hexagon-shape-controlled synthesis of graphene on copper surface. *Adv Mater* 23:3522–3525
- [39] Mohsin A, Liu L, Liu P, Deng W, Ivanov IN, Li G, Dyck EO, Duscher G, Dunlap RJ, Xiao K, Gu G (2013) Synthesis of millimeter-size hexagon-shaped graphene single crystals on resolidified copper. *ACS Nano* 7:8924–8931
- [40] Ma T, Ren W, Zhang X, Liu Z, Gao Y, Yin L, Ma X, Ding F, Cheng H (2013) Edge-controlled growth and kinetics of single-crystal graphene domains by chemical vapor deposition. *Proc Natl Acad Sci USA* 110:20386–20391
- [41] Yu Q, Jauregui LA, Wu W, Colby R, Tian J, Su Z, Cao H, Liu Z, Pandey D, Wei D, Chung TF, Peng P, Guisinger NP, Stach EA, Bao J, Pei S, Chen YP (2011) Control and characterization of individual grains and grain boundaries in graphene grown by chemical vapour deposition. *Nat Mater* 10:443–449
- [42] Wu B, Geng D, Xu Z, Guo Y, Huang L, Xue Y, Chen J, Yu G, Liu Y (2013) Self-organized graphene crystal patterns. *NPG Asia Mater* 5:e36
- [43] Simonov KA, Vinogradov NA, Vinogradov AS, Generalov AV, Zagrebina EM, Mårtensson N, Cafolla AA, Carpy T, Cunniffe JP, Preobrajenski AB (2014) Effect of substrate chemistry on the bottom-up fabrication of graphene nanoribbons: combined core-level spectroscopy and STM study. *J Phys Chem C* 118:12532–12540

- [44] Kimouche A, Ervasti MM, Drost R, Halonen S, Harju A, Joensuu PM, Sainio J, Peter L (2015) Ultra-narrow metallic armchair graphene nanoribbons. *Nat Commun* 6:10177
- [45] Jordan RS, Li YL, Lin C, McCurdy RD, Lin JB, Brosmer JL, Marsh KL, Khan SI, Houk KN, Kaner RB, Rubin Y (2017) Synthesis of N = 8 Armchair Graphene Nanoribbons from Four Distinct Polydiacetylenes. *J Am Chem Soc* 139:15878–15890
- [46] Cai J, Ruffieux P, Jaafar R, Bieri M, Braun T, Blankenburg S, Muoth M, Seitsonen AP, Saleh M, Feng X, Müllen K, Fasel R (2010) Atomically precise bottom-up fabrication of graphene nanoribbons. *Nature* 466:470–473
- [47] Chen X, Liu S, Liu L, Liu X, Wang L (2012) Growth of triangle-shape graphene on Cu(111) surface. *Appl Phys Lett* 100:163106
- [48] Wei E, Jin J, Wang Z, Lu Y, Wang L (2017) Spatially resolving and energy splitting of edge state in zigzag edged triangle graphene quantum dots on Cu(111) surface. *Phys E Low Dimens Syst Nanostruct* 89:10–14
- [49] Bronner C, Marangoni T, Rizzo DJ, Durr RA, Jørgensen JH, Fischer FR, Crommie MF (2017) Iodine versus bromine functionalization for bottom-up graphene nanoribbon growth: role of diffusion. *J Phys Chem C* 121:18490–18495
- [50] Chen Z, Zhang W, Palma CA, Rizzini AL, Liu B, Abbas A, Richter N, Martini L, Wang X, Cavani N, Lu H, Mishra N, Coletti C, Berger R, Klappenberger F, Kläui M, Candini A, Affronte M, Zhou C, Renzi VD, Pennino U, Barth JV, Räder HJ, Narita A, Feng X, Müllen K (2016) Synthesis of graphene nanoribbons by ambient-pressure chemical vapor deposition and device integration. *J Am Chem Soc* 138:15488–15496
- [51] Yang W, Lucotti A, Tommasini M, Chalifoux WA (2016) Bottom-up synthesis of soluble and narrow graphene nanoribbons using alkyne benzannulations. *J Am Chem Soc* 138:9137–9144
- [52] Narita A, Verzhbitskiy IA, Frederickx W, Mali KS, Jensen SA, Hansen MR, Bonn M, Feyter S, Casiraghi C, Feng X, Müllen K (2014) Bottom-up synthesis of liquid-phase-processable graphene nanoribbons with near-infrared absorption. *ACS Nano* 8:11622–11630
- [53] Suenaga K, Koshino M (2010) Atom-by-atom spectroscopy at graphene edge. *Nature* 468:1088–1090
- [54] Girit CO, Meyer JC, Erni R, Rossell MD, Kisielowski C, Yang L, Park CH, Crommie MF, Cohen ML, Louie SG, Zettl A (2009) Graphene at the edge: stability and dynamics. *Science* 323:1705–1708
- [55] Kim K, Coh S, Kisielowski C, Crommie MF, Louie SG, Cohen ML, Zettl A (2013) Atomically perfect torn graphene edges and their reversible reconstruction. *Nat Commun* 4:2723
- [56] Yamada Y, Murota K, Fujita R, Kim J, Watanabe A, Nakamura M, Sato S, Hata K, Peter E, Ciston J, Song C, Kim K, Regan W, Gannett W, Zettl A (2014) Subnanometer vacancy defects introduced on graphene by oxygen gas. *J Am Chem Soc* 136:2232–2235
- [57] Sasaki T, Yamada Y, Sato S (2018) Quantitative analysis of zigzag and armchair edges on carbon materials with and without pentagons using infrared spectroscopy. *Anal Chem* 90:10724–10731
- [58] Fuente E, Menéndez JA, Díez MA, Suárez D, Montes-Morán MA (2003) Infrared spectroscopy of carbon materials: a quantum chemical study of model compounds. *J Phys Chem B* 107:6350–6359
- [59] Yamada Y, Masaki S, Sato S (2020) Brominated positions on graphene nanoribbon analyzed by infrared spectroscopy. *J Mater Sci* 55:10522–10542. <https://doi.org/10.1007/s10853-020-04786-1>
- [60] Kanazawa S, Yamada Y, Sato S (2021) Infrared spectroscopy of graphene nanoribbons and aromatic compounds with sp<sup>3</sup>C-H (methyl or methylene groups). *J Mater Sci* 56:12285–12314. <https://doi.org/10.1007/s10853-021-06001-1>
- [61] Yamada Y, Gohda S, Abe K, Togo T, Shimano N, Sasaki T, Tanaka H, Ono H, Ohba T, Kubo S, Ohkubo T, Sato S (2017) Carbon materials with controlled edge structures. *Carbon* 122:694–701
- [62] Tommasini M, Lucotti A, Alfè M, Ciajolo A, Zerbi G (2016) Fingerprints of polycyclic aromatic hydrocarbons (PAHs) in infrared absorption spectroscopy. *Spectrochim Acta Part A Mol Biomol Spectrosc* 152:134–148
- [63] Diana N, Yamada Y, Gohda S, Ono H, Kubo S, Sato S (2021) Carbon materials with high pentagon density. *J Mater Sci* 56:2912–2943. <https://doi.org/10.1007/s10853-020-05392-x>
- [64] Eckmann A, Felten A, Mishchenko A, Britnell L, Krupke R, Novoselov KS, Casiraghi C (2012) Probing the nature of defects in graphene by raman spectroscopy. *Nano Lett* 12:3925–3930
- [65] Smith MW, Dallmeyer I, Johnson TJ, Brauer CS, McEwen JS, Espinal JF, Garcia-Perez M (2016) Structural analysis of char by Raman spectroscopy: improving band assignments through computational calculations from first principles. *Carbon* 100:678–692
- [66] Enoki T, Fujii S, Takai K (2012) Zigzag and armchair edges in graphene. *Carbon* 50:3141–3145
- [67] Kitao T, MacLean MWA, Nakata K, Takayanagi M, Nagaoka M, Uemura T (2020) Scalable and precise synthesis of armchair-edge graphene nanoribbon in metal-organic framework. *J Am Chem Soc* 142:5509–5514

- [68] Mazur AS, Vovk MA, Tolstoy PM (2020) Solid-state  $^{13}\text{C}$  NMR of carbon nanostructures (milled graphite, graphene, carbon nanotubes, nanodiamonds, fullerenes) in 2000–2019: a mini-review. *Fuller Nanotub Carbon Nanostruct* 28:202–213
- [69] de Souza FAL, Ambrozio AR, Souza ES, Cipriano DF, Scopel WL, Freitas JCC (2016) NMR spectral parameters in graphene, graphite, and related materials: ab initio calculations and experimental results. *J Phys Chem C* 120:27707–27716
- [70] He H, Riedl T, Lerf A, Klinowski J (1996) Solid-state NMR studies of the structure of graphite oxide. *J Phys Chem* 100:19954–19958
- [71] Kato T, Yamada Y, Nishikawa Y, Ishikawa H, Sato S (2021) Carbonization mechanisms of polyimide: methodology to analyze carbon materials with nitrogen, oxygen, pentagons, and heptagons. *Carbon* 178:58–80
- [72] Gohda S, Yamada Y, Murata M, Saito M, Kanazawa S, Ono H, Sato S (2020) Bottom-up synthesis of highly soluble carbon materials. *J Mater Sci* 55:11808–11828. <https://doi.org/10.1007/s10853-020-04813-1>
- [73] Yamada Y, Yasuda H, Murota K, Nakamura M, Sodesawa T, Sato S (2013) Analysis of heat-treated graphite oxide by X-ray photoelectron spectroscopy. *J Mater Sci* 48:8171–8198. <https://doi.org/10.1007/s10853-013-7630-0>
- [74] Yamada Y, Kim J, Matsuo S, Sato S (2014) Nitrogen-containing graphene analyzed by X-ray photoelectron spectroscopy. *Carbon* 70:59–74
- [75] Kato T, Yamada Y, Nishikawa Y, Otomo T, Sato H, Sato S (2021) Origins of peaks of graphitic nitrogen in N1s X-ray photoelectron spectra of carbon materials: quaternary or tertiary nitrogen? *J Mater Sci* 56:15798–15811. <https://doi.org/10.1007/s10853-021-06283-5>
- [76] Senda T, Yamada Y, Morimoto M, Nono N, Sogabe T, Kubo S, Sato S (2019) Analyses of oxidation process for isotropic pitch-based carbon fiber using model compounds. *Carbon* 142:311–326
- [77] Kim J, Yamada Y, Suzuki Y, Ciston J, Sato S (2014) Pyrolysis of epoxidized fullerenes analyzed by spectroscopies. *J Phys Chem C* 118:7076–7084
- [78] Kanazawa S, Yamada Y, Gohda S, Sato S (2021) Bottom-up synthesis of oxygen-containing carbon materials using a lewis acid catalyst. *J Mater Sci* 56:15698–15717. <https://doi.org/10.1007/s10853-021-06284-4>
- [79] Susi T, Pichler T, Ayala P (2015) X-ray photoelectron spectroscopy of graphitic carbon nanomaterials doped with heteroatoms. *Beilstein J Nanotechnol* 6:177–192
- [80] Yamada Y, Suzuki Y, Yasuda H, Uchizawa S, Hirose-Takai K, Sato Y, Suenaga K, Sato S (2014) Functionalized graphene sheets coordinating metal cations. *Carbon* 75:81–94
- [81] Yamada Y, Miyauchi M, Kim J, Takai KH, Sato Y, Suenaga K, Ohba T, Sodesawa T, Sato S (2011) Exfoliated graphene ligands stabilizing copper cations. *Carbon* 49:3375–3378
- [82] Fujimoto A, Yamada Y, Koinuma M, Sato S (2016) Origins of  $\text{sp}^3\text{C}$  peaks in C1s X-ray photoelectron spectra of carbon materials. *Anal Chem* 88:6110–6114
- [83] Susi T, Kaukonen M, Havu P, Ljungberg MP, Ayala P, Kauppinen EI (2014) Core level binding energies of functionalized and defective graphene. *Beilstein J Nanotechnol* 5:121–132
- [84] Kim J, Yamada Y, Kawai M, Tanabe T, Sato S (2015) Spectral change of simulated X-ray photoelectron spectroscopy from graphene to fullerene. *J Mater Sci* 50:6739–6747. <https://doi.org/10.1007/s10853-015-9229-0>
- [85] Kim J, Lee N, Choi DY, Kim DY, Kawai R, Yamada Y (2021) Pentagons and heptagons on edges of graphene nanoflakes analyzed by X-ray photoelectron and Raman spectroscopies. *J Phys Chem Lett* 12:9955–9962
- [86] Kim J, Han JW, Yamada Y (2021) Heptagons in the basal plane of graphene nanoflakes analyzed by simulated X-ray photoelectron spectroscopy. *ACS Omega* 6:2389–2395
- [87] Kelemen SR, Rose KD, Kwiatek PJ (1993) Carbon aromaticity based on XPS II to II\* signal intensity. *Appl Surf Sci* 64:167–173
- [88] Estrade-Szwarckopf E (2004) XPS photoemission in carbonaceous materials: a defect peak beside the graphitic asymmetric peak. *Carbon* 42:1713–1721
- [89] Smith M, Scudiero L, Espinal J, McEwen JS, Garcia-Perez M (2016) Improving the deconvolution and interpretation of XPS spectra from chars by ab initio calculations. *Carbon* 110:155–171
- [90] Gaussian 09, Revision A.02, Frisch MJ, Trucks GW, Schlegel HB, Scuseria GE, Robb MA, Cheeseman JR et al (2009) Gaussian 09, revision E.01. Gaussian Inc, Wallingford, CT
- [91] Kojima I, Fukumoto N, Kurahashi M (1986) Analysis of X-ray photoelectron spectrum with asymmetric Gaussian-Lorentzian mixed function. *Bunseki Kagaku* 35:T96-T100. [written in Japanese]
- [92] Solà M (2013) Forty years of Clar's aromatic  $\pi$ -sextet rule. *Front Chem* 1:1–8
- [93] Wu JB, Lin YF, Wang J, Chang PJ, Tasi CP, Lu CC, Chiu HT, Yang YW (2003) Correlation between N 1s XPS binding energy and bond distance in metal amido, imido, and nitrido complexes. *Inorg Chem* 42:4516–4518
- [94] Yamada Y, Tanaka H, Tanaka Y, Kubo S, Taguchi T, Sato S (2022) Toward strategical bottom-up synthesis of carbon materials with exceptionally high pyridinic-nitrogen content: development of screening techniques. *Carbon* 198:411–434. <https://doi.org/10.1016/j.carbon.2022.06.069>

- [95] Anno T, Ito M, Shimada R, Sado A, Mizushima W (1957) Relations among bond order, force constant and bond length for the C-C and the C-N bond in conjugated molecules. *Bull Chem Soc Jpn* 30:638–647
- [96] Han MY, Özyilmaz B, Zhang Y, Kim P (2007) Energy band-gap engineering of graphene nanoribbons. *Phys Rev Lett* 98:206805
- [97] Zarenia M, Chaves A, Farias GA, Peeters FM (2011) Energy levels of triangular and hexagonal graphene quantum dots: a comparative study between the tight-binding and Dirac equation approach. *Phys Rev B* 84:245403

**Publisher's Note** Springer Nature remains neutral with regard to jurisdictional claims in published maps and institutional affiliations.

Springer Nature or its licensor holds exclusive rights to this article under a publishing agreement with the author(s) or other rightsholder(s); author self-archiving of the accepted manuscript version of this article is solely governed by the terms of such publishing agreement and applicable law.